Real-Time Finger Force Estimation Robust to a Perturbation of Electrode Placement for Prosthetic Hand Control

Younggeol Cho and Pyungkang Kim

***Abstract*— In the use of real-time myoelectric controlled prostheses, the low accuracy of the user's intention estimation for simultaneous and proportional control (SPC) and the vulnerability to electrode shifts make application to real-world scenarios difficult. To overcome this barrier, we propose a method to estimate muscle unit activation in real time through neurophysiological modeling of the forearm. We also propose a high-performance finger force intention estimation model that is robust to perturbation of electrode placement based on estimated muscle unit activation. We compared the proposed model with previous studies for quantitative validation of finger force intention estimation and electrode shift compensation performance. Compared to other regression-based models in the on/offline test, our model achieved a significantly high intention estimation performance ($p < 0.001$). In addition, it attained high performance in electrode shift compensation, and at this time, the amount of data required and the number of models utilized were small. In conclusion, the model proposed in this study was verified to be robust to electrode shift and has high finger force intention estimation accuracy.**

***Index Terms*— Prosthetic hand, electromyogram (EMG), muscle activation, neurophysiological model, intention estimation, electrode shift compensation, rehabilitation.**

I. Introduction

IN ADDITION to the advancement of prosthetic hardware for rehabilitation and functional restoration of upper limb amputation patients, intention estimation algorithms for intuitive control of upper limb prostheses are being actively studied. Biosignal-based intention estimation algorithms can be divided into two types. The first is pattern recognition-based methods, which are adopted as control methods in commercial prostheses because they have high recognition accuracy and stability. Studies have classified hand and wrist motion using various pattern recognition techniques, such as common spatial pattern (CSP) [1], linear discriminant analysis (LDA) [2], and support vector machine (SVM) [3]. However, since only specific motions defined in advance are possible and simultaneous and proportional movement is difficult, intuitive prosthetic control is challenging [4].

The other type of intention estimation method is regression model-based algorithms, which are actively being considered in research and clinical trials. Such methods enable simultaneous and proportional control (SPC) by modeling the relationship between an electromyogram (EMG) and finger motion/force to overcome the limitations of pattern recognition and achieve more intuitive control of the prosthesis [5]. Model-based intention estimation algorithms can be divided into supervised and unsupervised learning approaches according to the model training method. Regarding supervised learning models, some studies have used the linear regression method (LR) [6] and the nonlinear method with an artificial neural network (ANN) [7]. Supervised learning-based models such as bilateral training [7] assume that both sides move or apply force equally. Performance differences occur according to the degree of development of both arms and the patient's ability.

In contrast, An unsupervised learning-based model is a method of generating a model without target data such as finger force and position. Linear models of unsupervised learning methods include nonnegative matrix factorization (NMF) and NMF using the Hadamard product (NMF-HP) [8]. Recently, a nonlinear model that enables simultaneous finger force intention estimation with high accuracy by reflecting the nonlinearity of the motor nervous system has been proposed [9]. This model showed high performance in estimating wrist force intention, and the authors emphasized the need for a nonlinear model. We proposed a new semi-unsupervised ANN that borrows only the structure of the autoencoder in a manner named the constrained autoencoder (CAEN) [10]. A learning method that maximizes the independence between fingers was proposed, and clinical tests showed high estimation accuracy in estimating finger force intention. CAEN is briefly described in the Methods section as part of the intention estimation model proposed in this paper. Previous SPC models have the following difficulties. Unlike the case of applying force to the wrist, the locations of the finger muscles are very close to each other (e.g. flexor digitorum profundus), and the EMG signal has high crosstalk. For this reason, in previous studies, as the number of estimated fingers increased, it was difficult to estimate intention in a situation where multiple fingers apply forces simultaneously.

Since the methods described above use only the magnitude of the surface EMG (sEMG) signal in the time and frequency domains, information loss occurs in the process of extracting

Manuscript received May 28, 2021; revised November 6, 2021 and April 13, 2022; accepted April 13, 2022. Date of publication April 29, 2022; date of current version May 16, 2022. This work was supported by the Basic Science Research Program through the National Research Foundation of Korea (NRF). *(Corresponding author: Pyungkang Kim.)*

This work involved human subjects or animals in its research. Approval of all ethical and experimental procedures and protocols was granted by the KAIST Bioethics Review Board under IRB Approval No. KH2018-95.

Younggeol Cho is with the Mechanical Engineering Department, Korea Advanced Institute of Science and Technology (KAIST), Daejeon 34141, South Korea (e-mail: younggeolcho@kaist.ac.kr).

Pyungkang Kim is with the Mechatronics Research and Development Center, Samsung Electronics, Hwaseong-si 18448, South Korea (e-mail: kimpyungkang@gmail.com).

Digital Object Identifier 10.1109/TNSRE.2022.3171394

the magnitude [11]. In addition, the intention estimation model of the existing regression method was created in the form of a training-based black box for the relationship between sEMG and finger force or position. This requires a large amount of training data and has limited performance in training situations. This is because the black box type model requires all EMG data acquired in a representative situation performed with prosthetic hands, and the performance of the model cannot be guaranteed in situations outside of the training data. Therefore, a performance decrease is caused by many factors, such as doffing and donning of a prosthetic hand, perturbation of electrode placement, change of muscle condition, and retraining.

To overcome the limitations of the preceding models and ensure high estimation accuracy and robustness of the model, a model based on muscle activity has recently been proposed [12]. The method estimates muscle unit activation from sEMG through a mathematical model based on neurophysiology, and the approach is applied to intention estimation. The muscle unit (MU) is the concept of a functional unit of a muscle and consists of alpha motor neurons and muscle fibers that are innervated by axons. Muscle activation is information expressed by the frequency of occurrence of action potentials that occur when each motor unit is activated by motor neuron stimulation [13]. The activity information of each muscle unit, not just the amplitude of the sEMG, can be used to develop an intention estimation model with high accuracy, and robustness can be ensured through parameter compensation. There was a study that estimated the joint angle of the wrist based on this muscle unit activation [14]. High-density sEMG was used, and the 3 degrees of freedom of the wrist joint angle were predicted using the spike train of the motor unit decoded through convolution kernel compensation (CKC). An LR model was used for intention estimation, and the possibility of prosthetic control using muscle activity was experimentally verified. However, in the CKC method using high-density sEMG, processing signals in real time is difficult due to the complexity of the model, so offline analysis was performed based on the acquired data. Some studies have shown that real-time estimation of the activation of a small number of muscle units is possible [15], but this information is difficult to use in estimating the real-time activity of a multimuscular unit for multidegree-of-freedom prosthetic control. There have been studies that estimate finger force or kinematics using motor unit activation. Motor unit spike trains (MUSTs) were decomposed from EMGs with blind-source separation based on CKC, and finger kinematics were estimated with high accuracy [16]. In another study, the superiority of neural information compared to the method using traditional EMG features such as root mean square (RMS) and slope sign changes was shown through finger force intention estimation results [17]. Another study showed that the use of motor unit driving information in the control of a prosthesis is better in terms of high intention estimation accuracy, fast response time, and smoothness of control [18].

A shift of the EMG electrode causes a decrease in the performance of the previous intention estimation models. Therefore, previous studies have been conducted to ensure robustness to electrode shifts. There are ways to extract features that are insensitive to electrode shifts and use them for intention estimation [19] or to retrain the model by acquiring data from multiple electrode shift situations [20]. Also, there was a study to reduce the effect of electrode shift using the transfer learning method [21]. All of these studies have shown their applicability to pattern recognition-based intention estimation methods. There is also a study applied to the SPC intention estimation method [22]. After acquiring EMG data according to wrist forces using high-density (HD)-EMGs, they ensured robustness by varying weights according to the sensitivity to electrode shifts. However, previous studies have not been validated in situations where crosstalk between EMG signals is severe, such as in estimating finger force intention, and a large number of electrodes are required. Additionally, the compensation results for the electrode shift in the muscle fiber direction were excellent, while the shift in the vertical direction was not completely compensated. This is because they tried to solve the problem by manipulating the acquired EMG signal, not by fundamentally compensating for the electrode shift in terms of the model. In contrast, we intend to present a model-based solution that compensates for the electrode position parameters in the model. To the best of our knowledge, none of the finger force intention estimation models have been robust to electrode movement in this way.

In this paper, we propose a finger force intention estimation model that is robust to electrode shift. The proposed model has three main features. By proposing a mathematical model for estimating muscle unit activation and using it for intention estimation, the finger force intention can be proportionally and simultaneously estimated with high accuracy. Real-time calculations are also possible. In addition, the robustness of the model is ensured via a compensation algorithm for the perturbation of electrode placement.

II. Methodology

A. Neurophysiological Modeling of an Electromyogram

The muscle unit action potential (MUAP) is expressed as the convolution of the fiber action potential and motor unit discharge timing within the unit.

$$MUAP(t) = u(t) * p(t) \tag{1}$$

p is the muscle fiber action potential, expressed as the sum of single fiber action potentials (ϕ_i) and formulated through a dipole model [23].

$$\phi_i(t) = \frac{I}{4\pi\sigma_z}\left(\frac{1}{r_{i,1}(t)} - \frac{1}{r_{i,2}(t)}\right) \tag{2}$$

$$r_{i,1}(t) = \sqrt{r_{i,f}^2 + z_e^2} = \sqrt{r_{i,f}^2 + (vt)^2} \tag{3}$$

$$r_{i,2}(t) = \sqrt{r_{i,f}^2 + (z_e + b)^2} = \sqrt{r_{i,f}^2 + (vt + b)^2} \tag{4}$$

The parameters in the formula are the dipole current (I), longitudinal conductivity (σ_z), conduction velocity (v), end plate-electrode distance (z_e), end plate-fiber termination ($L/2$). and $r_{i,1}$, $r_{i,2}$ are the distances from the electrode to the source and sink currents, respectively. $r_{i,f}$ is the radial distance from the electrode to fibers in i-th muscle unit.

The muscle fiber action potential (p) measured by the sEMG electrode is defined as the sum of the multiple fiber

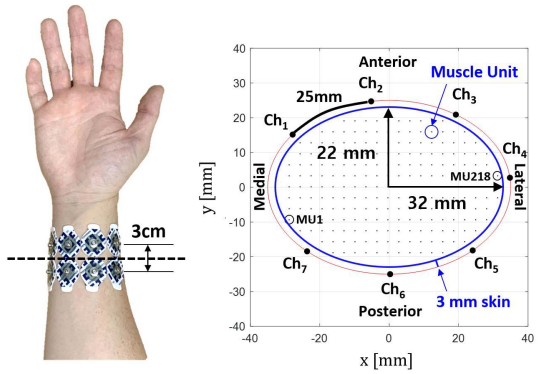

Fig. 1. Configuration of electrode placement. Seven electrode pairs were attached: four on the anterior and three on the posterior of the forearm. The graph is a cross-sectional model of the arm and includes electrode positions, arm cross-sectional shape and size, and muscle units. Muscle units are arranged at regular intervals and are represented by dots.

action potentials occurring in all muscle units and is expressed by the following formula.

$$p_{e,m}(t) = \sum_{i=1}^{N} \phi_{e,m,i}(t), (t = 0, 1, \ldots, L/v) \tag{5}$$

$\phi_{e,m,i}$ is the fiber action potential at the e-th sEMG electrode, the m-th muscle unit, and the i-th muscle fiber, and N is the number of fibers in each muscle unit.

u is the time of occurrence of the action potential of the fiber, expressed as a train in the form of a spike. The frequency of the occurrence of a muscle fiber action potential that occurs through induction of the motor nervous system indirectly indicates the activity of the muscle unit, which is formulated through the recruitment threshold excitation (RTE) [13] and interpulse frequency modulation (IPFM) [24] model. In this study, we propose a method to estimate muscle activation in real time based on sEMG signals and muscle unit action potentials.

B. Proposed Model: Estimation of Muscle Unit Activation

We propose a method to estimate muscle unit activation from an sEMG based on the above neurophysiological model. First, for the definition of the proposed model, the circumference of the arm where the sEMG signal was measured and the electrode attachment position, which are values that can be measured, are required. The circumference of the arm and the position of the electrode can be used to define the arm cross-section, as shown in Figure 1. The muscle units in the cross-section are arranged at regular intervals. The number of muscle units and muscle fibers are described in Experimental details.

In the EMG generation model produced through neurophysiology, the sEMG is the sum of the muscle unit activation potentials, and each muscle unit activation potential is expressed as the convolution of the muscle fiber action potential and the time of occurrence. The EMG generation model is expressed as a discrete approximation convolution equation as follows.

$$s_{e,m}(t) = \sum_{\tau=1}^{n} p_{e,m}(t-\tau)u_m(\tau) \tag{6}$$

$s_{e,m}$ is the sEMG signal obtained from electrode e at the mth muscle unit activation potential. $p_{e,m}$ is the unit activation potential in muscle unit m measured at electrode e, and u_m is the motor unit discharge timing in muscle unit m. n is the window length. We set the window length to 80 ms. This is because the muscle fiber conduction velocity is 4 m/s and the considered fiber length is 320 mm, so a window of at least 80 ms is required to obtain MUAPs. To ensure the real-time performance of the model, the discrete convolution equation is transformed into a matrix operation and expressed as follows.

$$\begin{bmatrix} p_{e,m}(t_1-\tau_1) & \cdots & p_{e,m}(t_1-\tau_n) \\ \vdots & \ddots & \vdots \\ p_{e,m}(t_T-\tau_1) & \cdots & p_{e,m}(t_T-\tau_n) \end{bmatrix} \begin{bmatrix} u_m(\tau_1) \\ \vdots \\ u_m(\tau_n) \end{bmatrix} = \begin{bmatrix} s_{e,m}(t_1) \\ \vdots \\ s_{e,m}(t_T) \end{bmatrix} \tag{7}$$

The defined matrix can be extended to all muscle unit activation potentials and all sEMG electrode signals and is expressed as follows.

$$P = \begin{bmatrix} P_{1,1} & \cdots & P_{1,M} \\ \vdots & \ddots & \vdots \\ P_{E,1} & \cdots & P_{E,M} \end{bmatrix}, U = \begin{bmatrix} U_1 \\ \vdots \\ U_M \end{bmatrix}, S = \begin{bmatrix} S_1 \\ \vdots \\ S_E \end{bmatrix} \tag{8}$$

Finally, the relationship of the convolution matrix of each muscle unit action potential P, the motor unit discharge timing matrix U representing muscle activity, and the sEMG signal matrix S obtained from each electrode is represented by a simple matrix product.

$$PU = S \tag{9}$$

S and P can be obtained by electrode measurements and a neurophysiological model of sEMG generation. Therefore, matrix U can be approximated via the Moore-Penrose inverse matrix as follows.

$$U = P^{+}S = (P^T P)^{-1} P^T S \tag{10}$$

P^{+} is the Moore-Penrose pseudoinverse matrix of matrix P and can be calculated as $(P^T P)^{-1} P^T$. Matrix U of all motor unit discharge timings can be obtained by multiplying the sEMG signal matrix S by the matrix P^{+}. Motor unit discharge timing is a discrete function with a value of 0 or 1, and the time interval of occurrence is inversely related to muscle activity. However, since matrix U calculated through the formula is calculated in an unconstrained situation, it takes a continuous value. In previous studies, the muscle activation approximation value was calculated with the active muscle unit activity frequency within a specific time window. In this study, the approximate value of muscle activation was estimated by applying the envelope filter. We also used all the estimated muscle unit activations to estimate finger force intentions.

C. Finger Force Intention Estimation Model Based on Muscle Activation

The CAEN model was used to estimate finger force intention using muscle unit activation. CAEN is a semi-unsupervised ANN, and a cost function has been defined

to maximize the independence between fingers. In a previous study, CAEN was able to estimate the simultaneous movement of fingers with high accuracy based on sEMG signals, and the approach improved the real-time control performance by ensuring independence between fingers. The CAEN described in reference [10] consists of input layer (U), 1st hidden layer (encoding layer, E), finger intention layer ($\hat{F}$), 3rd hidden layer (decoding layer, D), and output layer (U'). the calculation process of the CAEN is as follows.

$$\hat{F} = f_2(W^{\hat{F}} f_1(W^E U + b^E) + b^{\hat{F}}) \tag{11}$$

$$U' = W^U f_1(W^D \hat{F} + b^D) + b^U \tag{12}$$

$U \in R^{M \times T}$ is the muscle unit activation estimated based on the sEMG signal. In the encoding process (equation. 11), W^E and b^E are the weight and bias used to calculate the 1st hidden layer, $W^{\hat{F}}$ and $b^{\hat{F}}$ are the weight and bias used to calculate the finger force intention layer. f_1 is a rectified linear unit (RELU), and f_2 is the hyperbolic tangent function. In the decoding process (equation. 12), W^D and b^D are the weight and bias used to calculate the 3rd hidden layer, $W^{U'}$ and $b^{U'}$ are the weight and bias used to calculate the output layer. In defining the cost function, a constraint matrix C with the same dimension as $\hat{F}$ was defined as a label indicating the finger instructed to apply force when acquiring training data. C is a matrix indicating whether each finger is given strength during training. Each matrix element can take values of 0 or 1 as follows.

$$C = \begin{bmatrix} C_{Thumb,t_1} & C_{Thumb,t_2} & C_{Thumb,t_3} & \cdots \\ C_{Index,t_1} & C_{Index,t_2} & C_{Index,t_3} & \cdots \\ C_{Middle,t_1} & C_{Middle,t_2} & C_{Middle,t_3} & \cdots \end{bmatrix} = \begin{bmatrix} 1 & 0 & 0 & \cdots \\ 0 & 1 & 0 & \cdots \\ 0 & 0 & 1 & \cdots \end{bmatrix} \tag{13}$$

The cost function for training the CAEN model is as follows.

$$J = \left\| U - U' \right\|_2 + \frac{\left\| (1 - C)(\hat{F} \circ \hat{F}) \right\|_2}{\left\| C(\hat{F} \circ \hat{F}) \right\|_2} \tag{14}$$

The operator '$\circ$' is the Hadamard product, which multiplies the elements in the same position of two matrices with the same dimension. The cost function is the sum of the part that trains the input layer muscle unit activity U and the output layer U' equally and the part that maximizes the independence between the fingers while estimating the finger force intention. The denominator of the formula after the plus sign in the cost function only involves the node value of the finger that was instructed to apply the force through the Hadamard product of matrix C. In contrast, in the numerator, the matrix C in the denominator formula is changed to $1 - C$ so that only the node value of the finger that did not apply any force remains. Therefore, by minimizing the cost function, the finger force intention can be estimated with high interfinger independence by maximizing the finger force intention value for the finger applying the force and minimizing the rest.

D. Compensation of a Perturbation of Electrode Placement

Changes in electrode position inevitably occur depending on the time of use and removal of a prosthesis. In the case of the regression method of previous intention estimation models, acquisition of new training data and retraining of the model are inevitable, which requires time and effort from the user. To overcome this issue, in this study, the robustness of the model with respect to electrode position was ensured through an algorithm that compensates for electrode position change, which is one of the parameters in the proposed muscle unit activity estimation model. We performed compensation by changing the electrode position in the estimation model of muscle unit activation. The finger force estimation model, CAEN, does not change. The electrode position is a parameter that affects the muscle unit action potential P. Then, We can represent P^+ as a function of the electrode position from the equation.10.

$$U(s) = P^+(s)S \tag{15}$$

s is the shifted position based on the initial electrode position. Since CAEN is a model trained using the EMG acquired at the initial electrode position, the performance decreases when the electrode is shifted. When the electrode positions are shifted, we acquire EMG by grabbing three fingers and calculated $U(s)$ according to s. We define the cost function J including the muscle activity (U_o) of the same situation obtained at the initial electrode position.

$$J(s) = \left\| U(s) - U_o \right\|_2 \tag{16}$$

the compensation algorithm aims to find s such that the cost function J is minimized. This method can ensure robustness by modifying the parameters in the model without additional training data acquisition and model generation.

III. Experimental Details

A. Subjects

The subjects were 10 males, ranging in age from 24 to 33 years old. All subjects were right-handed, with intact hand function and no history of damage to the nervous system. The sEMG signal and fingertip force were acquired on the right arm of all participants. The experiment was approved by the KAIST Bioethics Review Board (IRB), and consent was obtained from all subjects after explaining the experimental process and precautions in detail.

B. Signal Acquisition and Experimental Protocol

Self-developed equipment was used to acquire and process sEMG signals. We obtained robust EMG using a differential amplifier (INA 128, Texas Instruments), a bandpass filter, and a right leg driver (RLD) circuit. The RLD is a circuit used to actively remove external electrical interference and common noise. The common-mode voltage obtained through an additional electrode for the RLD attached to the body is passed through an inverting amplifier and input to the differential amplifier. This allows active cancellation of common noise components acquired by the subject's body. A disposable electrode (Ag/AgCl, Kendall) was used as the sEMG electrode.

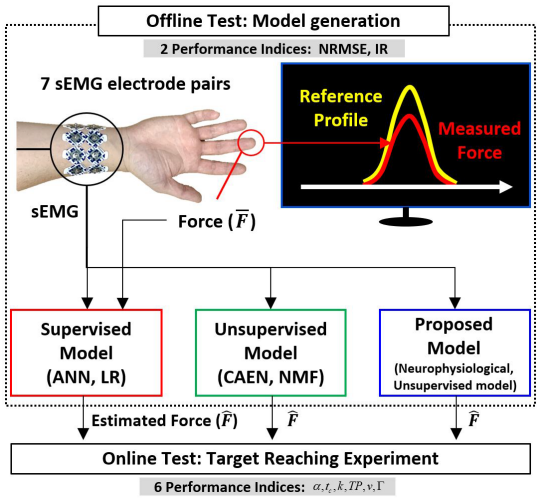

Fig. 2. Schematic diagram of the experimental protocol.Subjects look at the reference profile displayed on the monitor and apply force to fingers to match the measured force signal. At this time, EMG and finger force are recorded. Five models are created and analyzed performance using two indicators, the NRMSE and IR. An online test is conducted, and the results are analyzed using six indicators.

Electrodes were attached to the surface of the forearm close to the wrist with 7 channels (4 channels on the anterior and 3 channels on the posterior of the forearm) at 25 mm intervals, excluding the area close to the radius and ulna. The sEMG acquired through each channel passed through a signal amplification and filter circuit, and a signal was acquired by a desktop computer through a data acquisition (DAQ) board (Pcie-6363, National Instruments). A second-order infinite impulse response (IIR) Butterworth bandpass filter was applied to separate the signal obtained through the analog filter from the 5 – 500 Hz signal, which is the main frequency domain of the EMG. In the case of the preceding comparison model, a 1.5 Hz IIR Butterworth low-pass filter was applied to envelop the signal. Load cells (CBFS-10 K C-type, Bongshin Loadcell Co., Ltd.) were used to measure the force of the fingertips to obtain training data for the supervised learning method comparison model and to define the performance index of the intention estimation model. The signal was acquired with a 2 kHz sampling frequency, and the preceding signal processing was performed identically in all sEMG channels.

For data acquisition, a method similar to that used in previous studies was chosen for comparison with the preceding model, as shown in Figure 2. After attaching the sEMG electrode, the arm was placed in a comfortable position, and the sEMG and fingertip force were measured while applying force to each finger individually and simultaneously. The measurement was repeated five times for each type of force applied to each finger, and a total of 35 data acquisition processes were conducted. We displayed the subject's fingertip force obtained through the load cell on the monitor. The load cell signal was normalized based on the subject's maximum voluntary contraction (MVC). In addition, 1.5 seconds at the beginning and end of the ten-second interval were set as rest times, and the guide profile in the form of a sine wave was displayed along with the load cell signal for 7 seconds. The amplitude of the sine was selected as 50% of the MVC. The subject looked at the profile and applied force to the fingertip to follow the load cell signal, and at this time, the EMG signal was acquired.

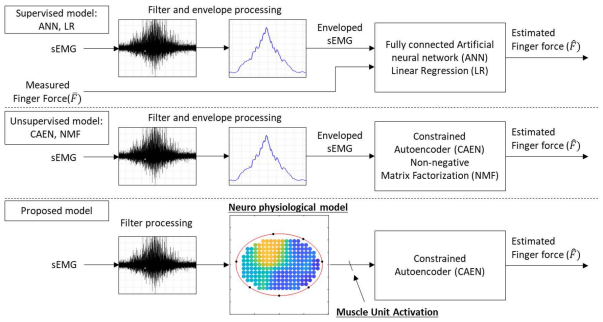

Fig. 3. Schematic diagram of the proposed model and comparative model. Supervised learning-based models (LR, ANN) were generated using EMG signals and fingertip force information, and unsupervised learning-based models (NMF, CAEN) were generated using only EMG signals. The comparative models were created based on the enveloped sEMG signal, but the proposed model estimated muscle activation based on the neurophysiological model using the EMG signal itself.

C. Offline Test: Model Generation

A schematic diagram of the proposed model and comparison model is shown in Figure 3. To create the proposed model, the number and position of muscle units in the cross-section of the arm and the position of the sEMG electrodes are defined. Depending on the size of the muscle, the number of muscle units and the number of muscle fibers in each muscle unit were calculated using the values cited in previous studies [13], [25]. We assumed that the muscle cross-section was an ellipse with the semi-major axis of 35 mm and the semi-minor axis of 25 mm, and the thickness of the skin was assumed to be 3 mm according to reference [26]. The same muscle cross-section assumption was applied to all subjects, and electrodes were attached to each subject's upper limb by finding the location most similar to the circumference of the ellipse. We arranged the muscle units to be equally spaced inside the muscle cross-section except for the skin. We performed a preliminary test to select the number of Muscle units as a hyper parameter. Performance change is insignificant at more than two hundred MUs, so we selected 218 MUs to secure real-time performance considering computation cost. The total number of muscle fibers was 44234, calculated based on the muscle area ($\pi * (32) * (22) mm^2$) and fiber density (20 $fibers/mm^2$). We assumed that the number of fibers in each MU had an exponential distribution based on the reference [13], and the formula is as follows.

$$nf_i = \alpha * e^{-\beta * i} \tag{17}$$

$$\alpha = (1 - e^{-\beta})/(1 - e^{-1}) * N_f \tag{18}$$

nf_i is the number of fibers in i-th MU and i is the MU number. β is the attenuation slope set to 1/218 in this study and is a value determined empirically as a hyper parameter. N_f is the total number of muscle fibers. Then, the convolution matrix P of the muscle unit action potential was calculated using the distance between the position of each muscle unit and the sEMG electrodes and the number of fibers in the muscle unit. The parameters taken from previous papers are shown in Table I [23].

After constructing matrix S using the measured sEMG signals, the activation of each muscle unit was estimated through the proposed model. CAEN was trained based on the estimated muscle unit activation. Data for model generation

TABLE I
PARAMETERS FOR THE MUSCLE ACTIVATION MODEL

Parameter	Symbol	Assigned Value
End plate-electrode distance	z_e	40 mm
End plate-fiber termination	$L/2$	120 mm
Dipole current	I	388 ηA
Dipole spacing	b	1 mm
Conduction velocity	v	4 m/s
Radial conductivity	σ_r	0.063 $mhos/m$
Longitudinal conductivity	σ_z	0.33 $mhos/m$

were acquired five trials for all combinations of finger force. Four out of five datasets (80%) were used as training data, and the remaining dataset (20%) was used as test data. The training process was conducted in 5-fold manner. In addition, since the model was trained in the mini-batch method after randomly shuffling the training data, the influence of the model performance according to the order of finger combination was minimized. During training, training data were randomly mixed and divided by 1/100 to perform minibatch learning, and the training termination condition was defined as follows. The independence ratio (IR) of the finger's estimated force intention value for each epoch was calculated, and we calculated the gradient of the change in the current IR value compared to the previous epoch. We stopped training when the gradient value was less than 0.1 for five epochs. The maximum number of epochs was set to 100. For verification through performance comparison, comparative intention estimation models were created. Among the preceding models, supervised learning-based models (LR, ANN) were trained using sEMG signals and measured fingertip force information, and unsupervised learning-based models (NMF, CAEN) were trained using only sEMG signals.

The model performance was analyzed with respect to two performance indicators. First, the difference between the estimated finger force intention value ($\hat{F}$) and the measured finger tip force (F) was defined as the normalized root mean square error (NRMSE), as follows.

$$NRMSE = \left\| F - \hat{F} \right\|_2 \tag{19}$$

The other performance indicator was the independence ratio (IR), which represents the independent movement of each finger. The IR is defined as the average value of the unintentional finger force versus the intended finger force minus 1, and the closer the value is to 1, the more accurately the force of the intended finger is estimated.

$$IR = 1 - \frac{\left\| \hat{F}_{Unintended} \right\|_2}{\left\| \hat{F}_{Intended} \right\|_2} \tag{20}$$

D. Online Test: Real-Time Target Reaching Experiment

We conducted a target reaching experiment (TRE) to indirectly verify the real-time prosthetic control performance (see Fig. 4). This experiment was performed in previous studies [10], [27] and proceeded as followings.

The estimated finger force intention is normalized based on 50% maximum voluntary contraction (MVC) and expressed as the bar's position in three windows for each finger. The bars can move between 0 (rest) and 1 (50% MVC). Then,

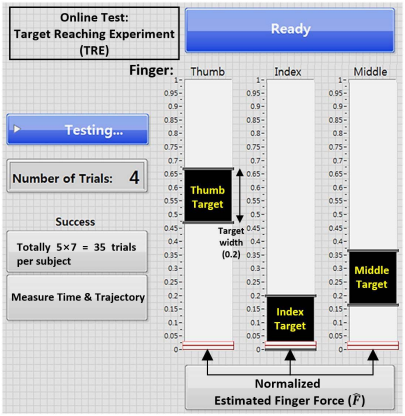

Fig. 4. Target reaching experiment (TRE). The estimated force intention of each finger is expressed as three bars, and the goal is to have the bars reach the black target windows simultaneously within the time limit.

TABLE II
ONLINE CONTROL PHASE PERFORMANCE INDICES

Performance Indices	Explanation
Completion rate (α, [%])	The number of completed trials / Total trials
Completion time (t_c, [s])	The time to complete a trial
Overshoots (k)	The number of red bar crosses of the target
Throughput (TP, [bit/s])	Task difficulty / t_c
Speed (v, [$1/s$])	Trajectory length / t_c
Efficiency coef (Γ,[%])	Optimal trajectory/ Actual trajectory

we marked the target in the form of a black box with a width of 0.2 [a.u.] in the three windows. The subjects should try to keep all bars within the target simultaneously. Subjects performed a total of 35 tasks involving targets in different positions for all instances of force on individual (T, I, M) and simultaneous (TI, TM, IM, TIM) fingers. A maximum of 20 seconds was given for one task, and beyond that, it was recorded as a failure. Ten seconds of rest was given between each task to allow the muscles to return to rest. To minimize the effect of user learning, the experimental order of the five models was randomly set, and the participants were not informed. In addition, In order to minimize the effect of muscle fatigue, we gave the subjects enough rest before testing with each model.

The results of the TRE were analyzed with respect to six performance indicators. During the TRE, the sEMG signal and the intention estimation trajectory for each finger were recorded. The completion rate (α), completion time (t_c), overshoot (k), throughput (TP), speed (v), and efficiency coefficient (Γ) were used as performance indicators. The definition of each performance index is provided in Table II.

E. Experiment for Compensation of the Perturbation of Electrode Placement

After shifting the positions of all electrodes by 25 mm, quantitative analysis was performed using the cost function (Equation 16), which defined the difference in activation of each MU before and after electrode shift. We selected previous methods for electrode position compensation to compare and verify the performance of the proposed method. First, there is

the group training (GT) method that trains a model using data acquired from multiple electrode location sites [28]. There is also the position identification (PI) method, which makes a model for each electrode position and selects a suitable model for use [29]. Offline analysis of 10 participants was performed, and we compared the performance of the model trained on the original electrode site when the electrode was moved but no compensation method was applied (shift) and when the GT, PI, and proposed methods were applied. We used CAEN as the finger force intention estimation model and analyzed it through the NRMSE and IR performance indicators. Additionally, after analyzing the offline results of ten participants, an online test was performed on two of them. We analyzed the performance change of five intention estimation models before and after electrode shift through online testing. All experimental conditions were the same, except for the electrode position.

F. Statistics

In this study, one-way repeated-measures ANOVA was performed to compare the performance between models. To determine the suitability of the statistical analysis assumptions, normality was first assessed by the Kolmogorov-Smirnov (KS) test. The assumption of homodispersity was verified by Levene's test, and the assumption of sphericity was verified by Mauchly's test. In the case of insufficient sphericity of the sample, the degrees of freedom were corrected using the Greenhouse-Geisser correction. Statistical comparison of the performance of each model was performed using the Bonferroni post hoc test. In all analyses, statistical significance was indicated by a P value less than 0.05.

IV. Results

A. Offline Test Results

The offline test results were analyzed according to the previously defined performance indicators NRMSE and IR, as shown in Figure 5. One-way repeated-measures ANOVA based on the Greenhouse-Geisser correction indicated statistically significant differences ($p<0.001$) between models in terms of both the NRMSE and IR. Bonferroni post hoc tests were performed to compare models, and the results are expressed as stars on the graph. The proposed model had a higher NRMSE than that of ANN but a lower NRMSE than the rest of the models. For the IR, which represents the independence between fingers, the proposed model outperformed ($p<0.001$) all other models. The average IR of the proposed model was 0.936, which is considerably higher than that of the other models (ANN: 0.883, CAEN: 0.920, LR: 0.777, NMF: 0.708). The intention estimation results are expressed as a graph in Figure 6. A high IR means that force can be applied to a finger independently during prosthetic control, which could lead to excellent results in the online TRE test.

B. Online Test Results

In online testing(see. fig. 7), the proposed model showed the highest performance on four of the six performance indicators (completion rate, completion time, throughput, and efficiency coefficient). In the case of success rate, the proposed model showed a statistically significant difference ($p<0.001$) from

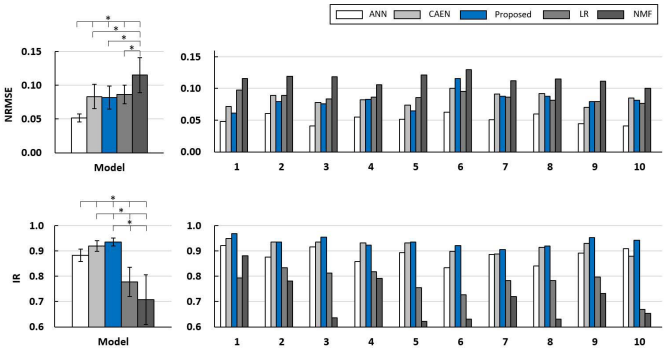

Fig. 5. Offline test results. The proposed model showed a low NRMSE compared to that of the previous models, except for the supervised learning nonlinear model ANN, and a high IR compared to all previous models.

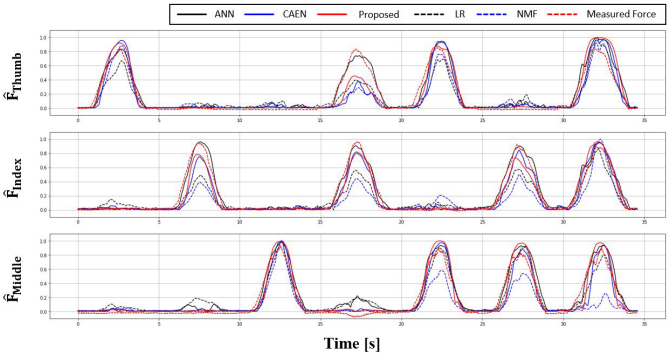

Fig. 6. Trajectory of finger force intention estimation over time. The measured finger force (red dashed line) and estimation results using five models are presented. The results of applying force in the order of type (T, I, M, TI, TM, IM, TIM) are shown. Compared to the linear models (LR, NMF), the proposed model has a small difference in the measured force trajectory. The proposed model maintains an estimated value close to zero in a situation where no force is applied, resulting in high independence between the fingers.

LR and NMF and achieved the highest value among all models. In terms of success time, the proposed model was fast, with a statistically significant difference ($p<0.001$) from ANN, LR, and NMF. In terms of overshoot, the performance was similar to that of the other models, except for ANN. In terms of throughput, the proposed model showed a statistically significant difference ($p<0.001$) from LR and NMF and achieved the highest value among all models. In terms of speed, the proposed model was fast, with a statistically significant difference ($p<0.001$) from LR and NMF but similar value to that of the nonlinear model. Finally, in terms of trajectory efficiency, the proposed model showed a statistically significant difference ($p<0.001$) compared to all other models and achieved the best performance. Detailed offline and online test results are shown in Table III.

C. Experimental Results of Compensation for the Perturbation of Electrode Placement

To verify the robustness of the proposed model against electrode position changes, the performance changes of all models before and after shifting the electrodes by 25 mm were analyzed. The cost function (Equation 16) calculated by

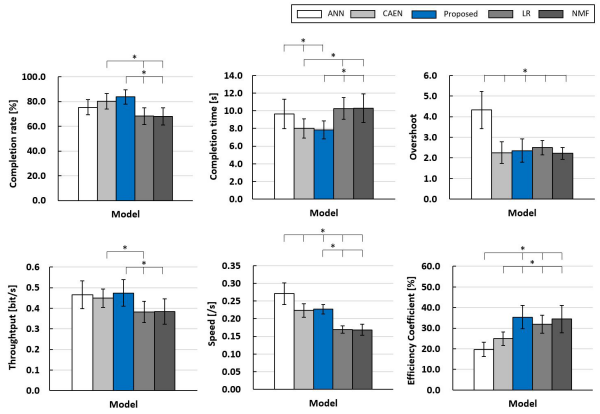

Fig. 7. Online test results according to 6 performance indicators. The proposed model outperformed the other models with respect to 4 performance indicators (completion rate, completion time, throughput, and efficiency coefficient).

TABLE III
OFFLINE/ONLINE TEST RESULTS

Indices	ANN	CAEN	Proposed	LR	NMF
NRMSE	0.051±0.006	0.083±0.018	0.082±0.017	0.086±0.014	0.115±0.026
IR	0.883±0.025	0.920±0.022	0.936±0.016	0.777±0.058	0.708±0.098
Comp. rate	75.43±6.10	80.29±6.27	83.71±5.72	68.29±6.77	68.00±7.02
Comp. time	9.63±1.66	8.01±1.08	7.83±1.03	10.26±1.23	10.30±1.62
Overshoots	4.32±0.91	2.25±0.53	2.35±0.57	2.50±0.35	2.22±0.29
Throughput	0.47±0.07	0.45±0.05	0.47±0.06	0.38±0.05	0.38±0.06
Speed	0.27±0.03	0.22±0.02	0.23±0.01	0.17±0.01	0.17±0.02
Efficiency	19.64±3.46	24.90±3.33	35.36±5.65	31.97±4.33	34.43±6.62

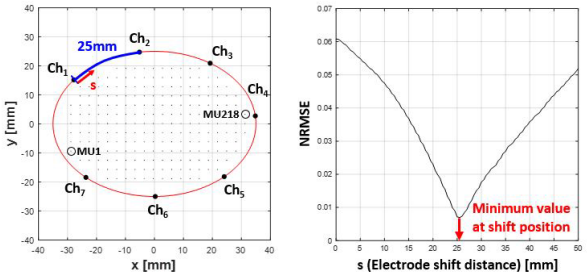

Fig. 8. Cost function trajectory according to the compensation of electrode position change. When the electrode was moved 25 mm after the initial model creation, the minimum value was achieved at approximately 25 mm, indicating the correct operation of the electrode position compensation algorithm.

the electrode position compensation algorithm of the proposed model according to the electrode position change in the model is expressed in Figure 8. The cost function when moving the electrode 25 mm is expressed as a graph, changing from the case where the position of the electrode in the model was not compensated (0 mm) to a maximum of 50 mm. At approximately 25 mm, the cost function showed the minimum value, which corresponds to an actual physical electrode position change of 25 mm. More intuitive analysis is possible by viewing the electrode position compensation results for each muscle unit. The graph on the left side of Figure 9 expresses the cost function for each muscle unit position in the arm

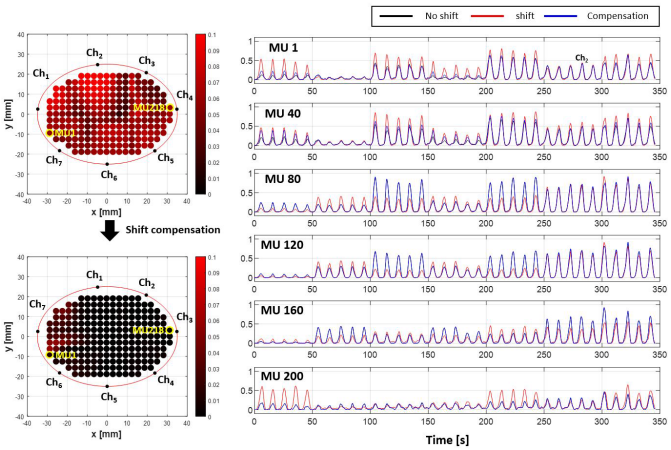

Fig. 9. Graphical representation of muscle unit activation for compensation of electrode position changes. The left graph shows the cost function value of each muscle unit before (top graph) and after (bottom graph) electrode position shift compensation. The closer the result is to the red color, the more severe the distortion of the muscle unit activity when the electrode position is shifted, and black indicates the same estimation as the muscle unit activity when the model is created. The graph on the right shows muscle unit activation before and after electrode position compensation in 6 muscle units.

cross-section before (upper left) and after (lower left) electrode position compensation. The cost function represents an error in estimating muscle activation before and after the electrode position shift, and before electrode position compensation, it shows a high error in all muscle units. However, the error significantly decreases after electrode position compensation. The graph on the right side of Figure 9 expresses the activation of six muscle units as an example. Before the electrode position change, each muscle unit activation is represented by a black line, and after the 25 mm electrode position shift, the muscle activation (red line) is greatly distorted. However, after electrode position compensation, the muscle activity (blue line) is very similar to that before the electrode position change. Therefore, even though the electrode position has changed, the method performs similarly to the first time the prosthetic was worn.

We analyzed the performance of each compensation method after changing the electrode position based on all previously used performance indicators, and the results are shown in Figure 10. When the electrode shifted by 25 mm without compensation for the model trained on the original site, the NRMSE increased approximately 2 times, and the IR value was a negative value, showing an extreme performance decrease. When the GT method was applied, the performance improved compared to before compensation, but a significant decrease in performance was observed compared to before the electrode shift. When the PI method was applied, the performance was similar to that of the original site model with a difference of less than 6% for the NRMSE and less than 1% for the IR. Similarly, the proposed model showed a less than 1% performance difference from the original site model in terms of the NRMSE and IR. That is, the PI and proposed models were compensated to achieve the performance of the original model despite the extreme electrode movement by 25 mm.

PI and the proposed model are similar in terms of electrode shift compensation performance, and specific actions must

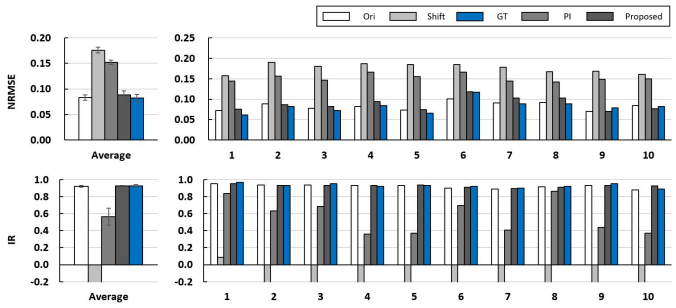

Fig. 10. Offline test results according to electrode position shift and compensation method. 'Shift' is the result after electrode shift without compensation. Additionally, the group training (GT), position identification (PI), and proposed method results are the results after electrode shift and compensation.

TABLE IV
CHARACTERISTICS OF ELECTRODE SHIFT COMPENSATION MODELS

Compensation method	GT	PI	Proposed
Number of models	One	Equal to the number of electrode sites	One
Amount of data for training models	Data of all sites	Data of all sites	Data of one site
Continuity of compensation	Discrete (Only at the location where the data were collected)	Discrete (Only at the location where the data were collected)	Continuous
Model selection or update strategy	No need	Requires data to perform specific actions	Requires data to perform specific actions
Performance compared to the original site	Decrease	Similar	Similar

be performed to select or update the model according to the electrode shift. However, there is a difference in the characteristics of the compensation method(see table. IV). PI requires as many models and training data as the number of electrode positions for which compensation is desired. In addition, since it is a discrete method that can compensate only for the position of the electrode for which the model is trained, a performance decrease is inevitable if it is out of that position. In contrast, the proposed model compensates only for the electrode position parameters so that model training is possible only with data obtained from the electrode position of the original site. In addition, the electrode position can be continuously compensated for. That is, the proposed method can compensate for the continuous electrode position shift with high performance using only one model.

In the online test experiment(see fig. 11), other models showed significant performance degradation compared to before electrode shift. The success rate decreased by more than 1/3 and was less than 25%, and the success time more than doubled. In addition, the overshoot increased by more than a factor of 2, and the trajectory efficiency decreased to 1/10 of the original value. However, for the proposed model, the performance before and after the electrode position change was similar for all performance indicators. The NRMSE and IR differed by less than 0.5%, and the online test results showed almost the same performance.

V. DISCUSSION

In this study, we proposed a method to estimate muscle unit activation from sEMG based on neurophysiology. Unlike

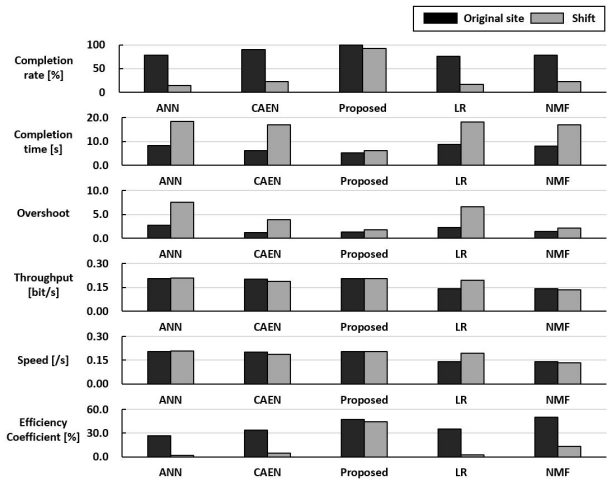

Fig. 11. Online test results of models after an electrode position shift. The averaged results of all participants are presented. In the case of the other models, the performance decreased significantly in all indicators, except for speed and throughput, but the proposed model maintained the performance in all indicators.

previous studies using EMG amplitude and time series feature extraction, the proposed method estimates fundamental muscle unit activation and uses it to estimate high-performance force intentions. In addition, the robustness of the model was verified through compensation for the electrode position. The robustness of the proposed model is due to the mathematical modeling of muscle units based on parameters, and similar approaches have previously been published [30], [31].

The proposed model was compared with previous models in offline/online tests. The online test ensured the reliability of the performance analysis by making the experimental configuration and verification method similar to those of previous studies [14], [27] related to intention estimation models. The proposed model outperformed previous models in terms of both the NRMSE and IR and achieved the best performance on four of the six performance indicators of the online test. Therefore, the proposed model has high competitiveness compared to previous models.

The robustness of the proposed model after an electrode position shift was also verified. We attempted to address the degradation in performance due to electrode shift, an issue solved in EMG-based prosthetic control through neurophysiological modeling. A quantitative comparison was performed with previous methods for compensating for electrode shift, and in offline tests, the proposed model was shown to be superior in terms of performance and amount of data (number of models) for compensation. In addition, the performance of the intention estimation model before and after the electrode shift was compared through an online test. When the compensation method was not applied, the previous model showed significant performance degradation in all performance indicators, but the proposed model showed similar performance even when using the intention estimation model trained at the original site by compensating for only the electrode position parameter. We performed an analysis of the extreme electrode shift situation of 25 mm due to hardware limitations, but additional analysis was also performed to indirectly show the performance of the proposed compensation method for electrode shifts of several millimeters that may occur in daily life.

TABLE V
CHARACTERISTICS OF ELECTRODE SHIFT COMPENSATION MODELS

	Shift distance[mm]	25	50	75	100	125	150
NRMSE[a.u.]	Uncompensated	0.060	0.076	0.077	0.075	0.071	0.054
	Compensated	0.007	0.014	0.020	0.020	0.015	0.007

We analyzed the situation in which all electrodes were moved sideways one channel at a time. This is an offline analysis of the data, and the results are shown in Table V.

When the electrode was shifted from 25 mm (one channel shift) to 150 mm (six channel shift), the proposed compensation method showed a high compensation performance with a less than 2% error from the original site performance in the estimation of muscle unit activation. Additionally, when the electrode shift is closer to the medial side, that is, the shift distance is small, the error after compensation tends to decrease. In other words, we can predict that the compensation performance will be higher in the electrode shift of a few millimeters that can occur in daily life.

In the electrode shift experiment, the previous models suffered significant performance decreases. So offline test was conducted with 10 subjects, but, the online test was conducted with only two subjects because the estimated force of the finger was substantially different from the intended force, which greatly increased the time for the online test experiment and made proceeding with the experiment difficult due to muscle fatigue and decreased concentration. We found a high correlation between offline and online test results, especially between IR and online test results. Therefore, we can suggest criteria for judging whether to conduct an online experiment based on the offline results. If the correlation coefficient between the offline performance indices before and after the electrode shift is below a certain level, then we can predict that the performance of the model is significantly reduced even if we do not proceed with the online experiment.

In this study, after acquiring EMG data of all channels, the electrode movement compensation algorithm was verified offline using the data shifted by one channel (the results are shown in Figs. 8 and 9). The results of the online test (Fig. 11) showed that it was actually a possible method for electrode position compensation but did not suggest a method to automatically detect the electrode position and update the model. In the future, we would like to propose a calibration method that provides compensation for the model by utilizing some representative hand movements. We will conduct a study to determine which representative motions provide good results in terms of time and electrode position compensation.

We used the estimated muscle unit activation for estimating finger force intention. We showed that the proposed model has robust characteristics to electrode movement. However, we expect the proposed model to be applicable to a wider field. The proposed method can acquire additional information called muscle unit activation. This allows us to monitor which upper limb muscles are contracting. Based on this muscle unit activation map, the degree of real-time muscle activity can be identified and used for rehabilitation. The proposed model can be used in the rehabilitation process to help amputees adapt to prosthetic limbs. It can also be used as information for rehabilitation guidance for patients with neurological abnormalities or patients who have undergone targeted muscle reinnervation surgery.

A. Limitations

The experimental and verification methods applied in this study have the following limitations. High-performance finger force intention estimation using the estimated muscle activity was possible, but the accuracy of the muscle activity estimation result was not verified. To overcome the limitations of the previous black box-type models, we proposed a mathematical model based on prior scientific reports. However, verification of the muscle activity estimation model itself was not carried out, and a neural network was used to estimate finger force intention. The results of this study must be compared with the results of previous studies [32] that estimated motor unit spike trains based on HD-EMGs or with direct measurements using internal EMGs. However, through this study, we proposed a gray box-type model that revealed a part of the neurophysiological process that gives strength to the fingers, and as a result, robustness characteristics were obtained according to the shift of the electrodes. An online test was conducted to verify its feasibility. In the future, we plan to conduct research that provides compensation by reflecting muscle fatigue, development and degeneration in the model.

One of the points to emphasize in the paper, the robustness of the intention estimation model, was analyzed by limiting the electrode position. Further research is needed to ensure robustness against other factors, such as muscle fatigue [33], development and degeneration and external stimulation [34]. In addition, all subjects are able-bodied: the results must be verified for amputees. The amplitude and frequency characteristics of the EMG change after amputation as muscle degenerates over time. Therefore, the results must be verified for amputees in various conditions. The experiment conducted in this study was analyzed in a situation where the arm movement was small and the object was not lifted. Performance verification is required in dynamic situations in which objects are moved or carried. We plan to evaluate and improve the model while performing real-life tasks by applying a robot prosthesis [35] that is currently under development.

VI. CONCLUSION

This study aimed to develop an intention estimation model based on the regression method using EMG signals in the clinical research stage. Most of the issues noted by previous research groups are related to the robustness of the model. Therefore, we obtained high accuracy and robustness of the model by performing mathematical modeling rather than implementing the conventional black box-type intention estimation model. The performance of the model was compared with four representative models. In the offline test, the proposed model showed high performance in intention estimation accuracy and independence between fingers. In the online test, the proposed model achieved the highest performance in 4 of 6 performance indicators.

The robustness of the proposed model was compared with that of previous models. After each electrode was shifted by 25 mm, the other models suffered significant performance degradation in offline/online test. But, the proposed model

maintained high performance. In conclusion, the proposed model has high performance and is robust to electrode position shifts. In future studies, we intend to develop a more robust model by applying the compensation technique to muscle fatigue and state changes. Finally, we intend to make the proposed intention estimation model practical for prosthetic arms of amputees and real-life applications.

REFERENCES

[1] W. Wu, X. Gao, and S. Gao, "One-versus-the-rest (OVR) algorithm: An extension of common spatial patterns (CSP) algorithm to multi-class case," in *Proc. IEEE Eng. Med. Biol. 27th Annu. Conf.*, Jan. 2005, pp. 2387–2390.

[2] A. Phinyomark, H. Hu, P. Phukpattaranont, and C. Limsakul, "Application of linear discriminant analysis in dimensionality reduction for hand motion classification," *Meas. Sci. Rev.*, vol. 12, no. 3, pp. 82–89, May 2012.

[3] M. Tavakoli, C. Benussi, P. A. Lopes, L. B. Osorio, and A. T. de Almeida, "Robust hand gesture recognition with a double channel surface EMG wearable armband and SVM classifier," *Biomed. Signal Process. Control*, vol. 46, pp. 121–130, Sep. 2018.

[4] A. J. Young, L. H. Smith, E. J. Rouse, and L. J. Hargrove, "Classification of simultaneous movements using surface EMG pattern recognition," *IEEE Trans. Biomed. Eng.*, vol. 60, no. 5, pp. 1250–1258, May 2013.

[5] J. M. Hahne, M. A. Schweisfurth, M. Koppe, and D. Farina, "Simultaneous control of multiple functions of bionic hand prostheses: Performance and robustness in end users," *Sci. Robot.*, vol. 3, no. 19, Jun. 2018, Art. no. eaat3630.

[6] L. H. Smith, T. A. Kuiken, and L. J. Hargrove, "Evaluation of linear regression simultaneous myoelectric control using intramuscular EMG," *IEEE Trans. Biomed. Eng.*, vol. 63, no. 4, pp. 737–746, Apr. 2016.

[7] J. L. Nielsen, S. Holmgaard, N. Jiang, K. B. Englehart, D. Farina, and P. A. Parker, "Simultaneous and proportional force estimation for multifunction myoelectric prostheses using mirrored bilateral training," *IEEE Trans. Biomed. Eng.*, vol. 58, no. 3, pp. 681–688, Mar. 2010.

[8] P. Kim, K.-S. Kim, and S. Kim, "Modified nonnegative matrix factorization using the Hadamard product to estimate real-time continuous finger-motion intentions," *IEEE Trans. Human-Mach. Syst.*, vol. 47, no. 6, pp. 1089–1099, Dec. 2017.

[9] I. Vujaklija, V. Shalchyan, E. N. Kamavuako, N. Jiang, H. R. Marateb, and D. Farina, "Online mapping of EMG signals into kinematics by autoencoding," *J. NeuroEngi. Rehabil.*, vol. 15, no. 1, pp. 1–9, Dec. 2018.

[10] Y. Cho, P. Kim, and K.-S. Kim, "Estimating simultaneous and proportional finger force intention based on sEMG using a constrained autoencoder," *IEEE Access*, vol. 8, pp. 138264–138276, 2020.

[11] K. G. Keenan, D. Farina, K. S. Maluf, R. Merletti, and R. M. Enoka, "Influence of amplitude cancellation on the simulated surface electromyogram," *J. Appl. Physiol.*, vol. 98, no. 1, pp. 120–131, Jan. 2005.

[12] D. Farina *et al.*, "The extraction of neural information from the surface EMG for the control of upper-limb prostheses: Emerging avenues and challenges," *IEEE Trans. Neural Syst. Rehabil. Eng.*, vol. 22, no. 4, pp. 797–809, Jul. 2014.

[13] A. J. Fuglevand, D. A. Winter, and A. E. Patla, "Models of recruitment and rate coding organization in motor-unit pools," *J. Neurophysiol.*, vol. 70, no. 6, pp. 2470–2488, Dec. 1993.

[14] T. Kapelner *et al.*, "Predicting wrist kinematics from motor unit discharge timings for the control of active prostheses," *J. NeuroEng. Rehabil.*, vol. 16, no. 1, p. 47, Apr. 2019.

[15] V. Glaser, A. Holobar, and D. Zazula, "Real-time motor unit identification from high-density surface EMG," *IEEE Trans. Neural Syst. Rehabil. Eng.*, vol. 21, no. 6, pp. 949–958, Nov. 2013.

[16] Y. Zheng and X. Hu, "Concurrent prediction of finger forces based on source separation and classification of neuron discharge information," *Int. J. Neural Syst.*, vol. 31, no. 6, Jun. 2021, Art. no. 2150010.

[17] C. Chen, G. Chai, W. Guo, X. Sheng, D. Farina, and X. Zhu, "Prediction of finger kinematics from discharge timings of motor units: Implications for intuitive control of myoelectric prostheses," *J. Neural Eng.*, vol. 16, no. 2, Apr. 2019, Art. no. 026005.

[18] M. D. Twardowski, S. H. Roy, Z. Li, P. Contessa, G. De Luca, and J. C. Kline, "Motor unit drive: A neural interface for real-time upper limb prosthetic control," *J. Neural Eng.*, vol. 16, no. 1, Feb. 2019, Art. no. 016012.

[19] L. Pan, D. Zhang, N. Jiang, X. Sheng, and X. Zhu, "Improving robustness against electrode shift of high density EMG for myoelectric control through common spatial patterns," *J. NeuroEng. Rehabil.*, vol. 12, no. 1, pp. 1–16, 2015.

[20] C. R. Steinhardt, J. Bettthauser, C. Hunt, and N. Thakor, "Registration of EMG electrodes to reduce classification errors due to electrode shift," in *Proc. IEEE Biomed. Circuits Syst. Conf. (BioCAS)*, Oct. 2018, pp. 1–4.

[21] A. Ameri, M. A. Akhaee, E. Scheme, and K. Englehart, "A deep transfer learning approach to reducing the effect of electrode shift in EMG pattern recognition-based control," *IEEE Trans. Neural Syst. Rehabil. Eng.*, vol. 28, no. 2, pp. 370–379, Feb. 2019.

[22] S. Muceli, N. Jiang, and D. Farina, "Extracting signals robust to electrode number and shift for online simultaneous and proportional myoelectric control by factorization algorithms," *IEEE Trans. Neural Syst. Rehabil. Eng.*, vol. 22, no. 3, pp. 623–633, May 2013.

[23] A. J. Fuglevand, D. A. Winter, A. E. Patla, and D. Stashuk, "Detection of motor unit action potentials with surface electrodes: Influence of electrode size and spacing," *Biol. Cybern.*, vol. 67, no. 2, pp. 143–153, Jun. 1992.

[24] E. J. Bayly, "Spectral analysis of pulse frequency modulation in the nervous systems," *IEEE Trans. Biomed. Eng.*, vol. BME-15, no. 4, pp. 257–265, Oct. 1968.

[25] S. Ma, C. Chen, D. Han, X. Sheng, D. Farina, and X. Zhu, "Subject-specific EMG modeling with multiple muscles: A preliminary study," in *Proc. 42nd Annu. Int. Conf. IEEE Eng. Med. Biol. Soc. (EMBC)*, Jul. 2020, pp. 740–743.

[26] M. A. Gibney, C. H. Arce, K. J. Byron, and L. J. Hirsch, "Skin and subcutaneous adipose layer thickness in adults with diabetes at sites used for insulin injections: Implications for needle length recommendations," *Current Med. Res. Opinion*, vol. 26, no. 6, pp. 1519–1530, 2010.

[27] N. Jiang, I. Vujaklija, H. Rehbaum, B. Graimann, and D. Farina, "Is accurate mapping of EMG signals on kinematics needed for precise online myoelectric control?" *IEEE Trans. Neural Syst. Rehabil. Eng.*, vol. 22, no. 3, pp. 549–558, May 2013.

[28] L. Hargrove, K. Englehart, and B. Hudgins, "A training strategy to reduce classification degradation due to electrode displacements in pattern recognition based myoelectric control," *Biomed. Signal Process. Control*, vol. 3, no. 2, pp. 175–180, 2008.

[29] J. He, X. Sheng, X. Zhu, and N. Jiang, "Position identification for robust myoelectric control against electrode shift," *IEEE Trans. Neural Syst. Rehabil. Eng.*, vol. 28, no. 12, pp. 3121–3128, Dec. 2020.

[30] T. Kapelner, M. Sartori, F. Negro, and D. Farina, "Neuromusculoskeletal mapping for man-machine interfacing," *Sci. Rep.*, vol. 10, no. 1, pp. 1–10, Dec. 2020.

[31] C. Chen, S. Ma, X. Sheng, D. Farina, and X. Zhu, "Adaptive real-time identification of motor unit discharges from non-stationary high-density surface electromyographic signals," *IEEE Trans. Biomed. Eng.*, vol. 67, no. 12, pp. 3501–3509, Dec. 2020.

[32] Y. Ning, X. Zhu, S. Zhu, and Y. Zhang, "Surface EMG decomposition based on K-means clustering and convolution kernel compensation," *IEEE J. Biomed. Health Inform.*, vol. 19, no. 2, pp. 471–477, Mar. 2014.

[33] M. Cifrek, V. Medved, S. Tonković, and S. Ostojić, "Surface EMG based muscle fatigue evaluation in biomechanics," *Clin. Biomech.*, vol. 24, no. 4, pp. 327–340, 2009.

[34] J. A. Spanias, E. J. Perreault, and L. J. Hargrove, "Detection of and compensation for EMG disturbances for powered lower limb prosthesis control," *IEEE Trans. Neural Syst. Rehabil. Eng.*, vol. 24, no. 2, pp. 226–234, Feb. 2015.

[35] S. H. Jeong, K.-S. Kim, and S. Kim, "Designing anthropomorphic robot hand with active dual-mode twisted string actuation mechanism and tiny tension sensors," *IEEE Robot. Autom. Lett.*, vol. 2, no. 3, pp. 1571–1578, Jul. 2017.